frontiers in Pharmacology

ORIGINAL RESEARCH
published: 07 May 2018
doi: 10.3389/fphar.2018.00313

The Metabolism of Separase Inhibitor Sepin-1 in Human, Mouse, and Rat Liver Microsomes

Feng Li[1,2,3], Nenggang Zhang[4,5], Siddharth Gorantla[4,5], Scott R. Gilbertson[6] and Debananda Pati[1,2,4,5]**

[1] Center for Drug Discovery, Baylor College of Medicine, Houston, TX, United States, [2] Department of Molecular and Cellular Biology, Baylor College of Medicine, Houston, TX, United States, [3] Advance Technology Core, Baylor College of Medicine, Houston, TX, United States, [4] Texas Children's Cancer Center, Houston, TX, United States, [5] Department of Pediatrics, Baylor College of Medicine, Houston, TX, United States, [6] Department of Chemistry, University of Houston, Houston, TX, United States

Separase, a known oncogene, is widely overexpressed in numerous human tumors of breast, bone, brain, blood, and prostate. Separase is an emerging target for cancer therapy, and separase enzymatic inhibitors such as sepin-1 are currently being developed to treat separase-overexpressed tumors. Drug metabolism plays a critical role in the efficacy and safety of drug development, as well as possible drug–drug interactions. In this study, we investigated the *in vitro* metabolism of sepin-1 in human, mouse, and rat liver microsomes (RLM) using metabolomic approaches. In human liver microsomes (HLM), we identified seven metabolites including one cysteine–sepin-1 adduct and one glutathione–sepin-1 adduct. All the sepin-1 metabolites in HLM were also found in both mouse and RLM. Using recombinant CYP450 isoenzymes, we demonstrated that multiple enzymes contributed to the metabolism of sepin-1, including CYP2D6 and CYP3A4 as the major metabolizing enzymes. Inhibitory effects of sepin-1 on seven major CYP450s were also evaluated using the corresponding substrates recommended by the US Food and Drug Administration. Our studies indicated that sepin-1 moderately inhibits CYP1A2, CYP2C19, and CYP3A4 with $IC_{50} < 10$ μM but weakly inhibits CYP2B6, CYP2C8/9, and CYP2D6 with $IC_{50} > 10$ μM. This information can be used to optimize the structures of sepin-1 for more suitable pharmacological properties and to predict the possible sepin-1 interactions with other chemotherapeutic drugs.

Keywords: separase inhibitor, liver microsomes, sepin-1 metabolism, CYP450 inhibition, metabolite identification

OPEN ACCESS

Edited by:
Yurong Lai,
Gilead (United States), United States

Reviewed by:
Panagiotis N. Moschou,
Swedish University of Agricultural Sciences, Sweden
John M. Rimoldi,
University of Mississippi, United States

****Correspondence:***
Feng Li
fl3@bcm.edu;
feng.li@bcm.edu
Debananda Pati
pati@bcm.edu

Specialty section:
This article was submitted to Drug Metabolism and Transport, a section of the journal Frontiers in Pharmacology

Received: *13 January 2018*
Accepted: *19 March 2018*
Published: *07 May 2018*

Citation:
Li F, Zhang N, Gorantla S, Gilbertson SR and Pati D (2018) The Metabolism of Separase Inhibitor Sepin-1 in Human, Mouse, and Rat Liver Microsomes. Front. Pharmacol. 9:313. doi: 10.3389/fphar.2018.00313

INTRODUCTION

Separase is an enzyme that resolves chromosomal cohesion and centriole engagement during mitosis. It is a cysteine protease in the CD clan (Uhlmann et al., 2000), with a catalytic domain structure similar to that of caspase (Viadiu et al., 2005; Winter et al., 2015; Lin et al., 2016). Although the N-terminus of separase varies, its C-terminus containing the proteolytic-active site is conserved

Abbreviations: CYP450, cytochrome P450; GEF, gefitinib; HLM, human liver microsomes; MLM, mouse liver microsomes; MRM, multiple-reaction monitoring; NADPH, nicotinamide adenine dinucleotide phosphate; OPLS-DA, orthogonal projection to latent structures-discriminant analysis; QQQMS, triple quadrupole mass spectrometry; QTOFMS, quadrupole time-of-flight mass spectrometry; RLM, rat liver microsomes; UHPLC, ultra-high performance liquid chromatography.

from yeast to humans (Zhang and Pati, 2017). The canonical role of separase in the cell cycle is to cleave cohesin Rad21 at the onset of anaphase to separate sister chromatids. Separase is also required for centrosome duplication by cleaving centrosomal Rad21 (Nakamura et al., 2009; Tsou et al., 2009; Schockel et al., 2011) and pericentrin/kendrin (Lee and Rhee, 2012; Matsuo et al., 2012) to disengage centrioles. In addition, separase is involved in DNA damage repair (Nagao et al., 2004; McAleenan et al., 2013) and vesicle trafficking (Bembenek et al., 2007; Richie et al., 2011; Moschou et al., 2013, 2016; Bai and Bembenek, 2017). Due to its importance in numerous cell processes, the activity of separate is tightly regulated (Ciosk et al., 1998; Zou et al., 1999; Stemmann et al., 2001; Gorr et al., 2005; Holland and Taylor, 2006). Notably, separase is overexpressed in many human cancers of breast, bone, brain, blood, and prostate (Pati, 2008; Meyer et al., 2009; Mukherjee et al., 2014a,b; Zhang and Pati, 2017). Overexpression of separase induces aneuploidy and tumorigenesis in mouse models (Zhang et al., 2008; Mukherjee et al., 2014b). Using a high-throughput screen, we have identified a novel small molecular inhibitor of separase, named sepin-1, which inhibits separase activity in a non-competitive way (Zhang et al., 2014). Sepin-1 selectively inhibits the growth of cancer cell lines including breast cancer, leukemia, and neuroblastoma. It also inhibits the growth of breast cancer xenografts in mice. Sepin-1 induces apoptosis and its effect on the inhibition of cell growth is positively correlated to the level of separase in the cancer cells and tumors (Zhang et al., 2014). It suggests that sepin-1 possesses a great potential to be used for cancer treatment, particularly to treat separase-overexpressed tumors. Additionally, the use of inhibitors could resolve the non-canonical functions of separase as well.

In drug development, a drug's metabolism plays a critical role in its efficacy and safety. As a preclinical evaluation of sepin-1, here we have profiled the Phase I metabolism and bioactivation of sepin-1 in HLM (Uhlmann et al., 2000), MLM, and RLM, using metabolomic approaches, which have been shown to be powerful tools for studying drug metabolism (Li et al., 2014; Liu et al., 2015, 2016). The metabolic enzymes contributing to the metabolism of sepin-1 were identified using recombinant CYP450s, and the possible reactive metabolites were investigated in HLM using glutathione (GSH) as the trapping agent. The inhibitory effects of sepin-1 on seven common CYP450s were also evaluated. These results can be used further to optimize the structures of sepin-1, resulting in more suitable pharmacological properties and reduced possible toxicity, as well as to predict the metabolism-mediated possible interactions of sepin-1 with other chemotherapeutic drugs.

MATERIALS AND METHODS

Materials

Sepin-1 (2,2-dimethyl-5-nitro-2H-benzimidazole-1,3-dioxide) with >97% purity was purchased from ChemBridge (San Diego, CA, United States). Phenacetin, efavirenz, paclitaxel, (*S*)-mephenytoin, quercetin, α-naphthoflavone, ticlopidine, ketoconazole, sulfaphenazole, and dextromethorphan were purchased from Cayman Chemical (Ann Arbor, MI, United States). Reduced GSH, diclofenac sodium, quinidine, midazolam solution, formic acid, and NADPH were obtained from Sigma-Aldrich (St. Louis, MO, United States). HLM, MLM, and RLM, and the recombinant human CYP450s (EasyCYP Bactosomes) were purchased from XenoTech (Lenexa, KS, United States). All the solvents for LC and MS were of the highest grade commercially available.

Metabolism of Sepin-1 in HLM, MLM, RLM, and Recombinant CYP450s

Incubations were conducted in 1× phosphate-buffered saline (1× PBS, pH 7.4), containing 30 μM sepin-1, 1.0 mg HLM, MLM, RLM, or 2 pmol of each cDNA-expressed P450 enzyme (control, CYP1A2, 2A6, 2B6, 2C8, 2C9, 2C19, 2D6, 2E1, and CYP3A4) in a final volume of 190 μl. After 5 min of pre-incubation at 37°C, the reaction was initiated by adding 10 μl of 20 mM NADPH (final concentration 1.0 mM) and continued for 30 min, with shaking at 37°C. Incubations lacking NADPH served as controls. Reactions were terminated with 200 μl of ice-cold methanol, followed by vortexing for 30 s and centrifuging at 15,000 × *g* for 15 min. Each supernatant was transferred to an auto sampler vial, and 5.0 μl was injected on to UHPLC coupled with a QTOFMS system for metabolite analysis. Incubations were conducted in quadruplicate for HLM, in triplicate for MLM and RLM, and in duplicate for cDNA-expressed P450 enzymes.

Trapping Reactive Metabolites Using Glutathione

The reactive metabolites were trapped with GSH in our current study. The experiments were conducted in 1× PBS (pH 7.4), containing 30 μM sepin-1, 1.0 mg HLM, and GSH (2.5 mM) in a final volume of 190 μl. After 5 min of pre-incubation at 37°C, the reactions were initiated by the addition of 10 μl of 20 mM NADPH (final concentration 1.0 mM) and continued for 30 min with gentle shaking. Incubations in the absence of NADPH and trapping agents were used as controls. The reactions were quenched by adding 200 μl of ice-cold methanol. The mixtures were vortexed for one 30 s and centrifuged at 15,000 × *g* for 15 min. The supernatants were transferred to sample vials for analysis. Incubations were performed in triplicate.

Inhibition of Sepin-1 on CYP450s

Incubations were performed in 1× PBS (pH 7.4), containing 0, 0.156, 0.312, 0.625, 1.25, 2.5, 5, 10, 20, or 40 μM sepin-1, 2 pmol of each cDNA-expressed P450 enzymes, and corresponding substrates: CYP1A2 (phenacetin, 40 μM, 20 min incubation), 2B6 (efavirenz, 20 μM, 30 min), 2C8 (paclitaxel, 10 μM, 30 min), 2C9 (diclofenac, 5 μM, 15 min), 2C19 [(*S*)-mephenytoin, 40 μM, 20 min], 2D6 (dextromethorphan, 5 μM, 15 min), and CYP3A4 (midazolam, 3 μM, 10 min) in a final volume of 190 μl. After 5 min of pre-incubation at 37°C, the reaction was initiated by adding 10 μl of 20 mM NADPH (final concentration 1.0 mM) and continued for a specific time as presented above with gentle shaking. Incubations without sepin-1 were used as controls. Reactions were terminated by the addition of 200 μl

of ice-cold methanol, vortexing for 30 s, and centrifuging at 15,000 × *g* for 15 min. Each supernatant was transferred to an auto sampler vial and 5.0 μl was injected on to UHPLC coupled with a QQQMS system for the specific metabolite analysis. A MRM method was used. Incubations were conducted in duplicate. Positive controls were performed by using a known specific inhibitor for each of the isoform assays (Supplementary Table S1).

UHPLC–QTOFMS Analyses

The separation of sepin-1 and its metabolites was achieved using a 1260 Infinity Binary LC System (Agilent Technologies, Santa Clara, CA, United States) equipped with 100 mm × 2.1 mm (Agilent XDB C18) column. The column temperature was maintained at 40°C. The flow rate was 0.3 ml/min, with a gradient ranging from 2% to 98% aqueous acetonitrile containing 0.1% formic acid in a 15-min run. QTOFMS was operated in a positive mode with electrospray ionization. Ultra-high pure nitrogen was applied as the drying gas (12 l/min) and the collision gas. The drying gas temperature was set at 325°C, and the nebulizer pressure was kept at 35 psi. The capillary voltages were set at 3.5 kV. During MS, real-time mass correction and accurate mass were achieved by continuously measuring standard reference ions at *m/z* 121.0508 and 922.0098 in the positive mode. The MS/MS of sepin-1 metabolites was performed in a targeted mode with a default isolation width of *m/z* 4 and collision energy ramp ranging from 10 to 45 V.

UHPLC–QQQMS Analyses

The separations of each enzyme substrate and its specific metabolite were achieved using a 1260 Infinity Binary LC System (Agilent Technologies, Santa Clara, CA, United States) equipped with the 50 mm × 4.6 mm (Agilent XDB C18). The flow rate was 0.3 ml/min, and the mobile phases were water and acetonitrile with 0.1% formic acid. QQQMS was operated in a positive mode with electrospray ionization. Ultra-high pure nitrogen was applied as the drying gas (14 l/min) and the collision gas. The drying gas temperature was set at 280°C and the nebulizer pressure was kept at 20 psi. The capillary voltages were set at 3.6 kV for positive mode and 3.0 kV for negative mode. The MRM transitions for the specific metabolites are listed in **Table 1**. The second transitions were used for confirmation purposes.

Data Analysis

Mass chromatograms and mass spectra were acquired by MassHunter Workstation Data Acquisition Software (Agilent, Santa Clara, CA, United States) in centroid and profile formats from *m/z* 100 to 1000. The acquisition rate was set as 1.5 spectra per second. Centroid and integrated mass chromatographic data were processed by Mass Profinder and Mass Profiler Professional Software (Agilent, Santa Clara, CA, United States) to generate a multivariate data matrix. The corresponding data matrices were then exported into SIMCA13 (Umetrics, Kinnelon, NJ, United States) for multivariate data analysis. OPLS-DA was conducted on Pareto-scaled data. For the QQQMS data, QQQ Quantitative Analysis Software (Agilent, Santa Clara, CA, United States) was used for metabolite analysis. For chemometric analysis, matrix data were processed from *m/z* 50 to 600. The experimental data are presented as mean ± SEM. Statistical differences between two groups were determined by Student's *t*-test.

RESULTS

Profiling of Sepin-1 Metabolism in HLM Using a Metabolomic Approach

The results of metabolomic analysis on the ions generated from UHPLC–QTOFMS analysis of control and sepin-1 group are shown in Supplementary Figure S1. Metabolomic analysis unraveled two clusters (Supplementary Figure S1A) corresponding to the control and sepin-1 group in the score plots, which indicated the chemical components are different between control and sepin-1 groups. The S-plot generated from OPLS-DA displays ion contribution to group separation in HLM (Supplementary Figure S1B). The top ranking ions were identified as sepin-1 metabolites, which were marked with M1-6 in the S-plot (Supplementary Figure S1B). The majority of the sepin-1 metabolites in HLM were also found in MLM and RLM (**Figure 1**). The information associated with sepin-1 metabolites is summarized in **Table 1**. The relative abundance of metabolites in HLM, MLM, and RLM is presented in **Figure 1**. Overall, seven sepin-1 metabolites and adducts, including one cysteine–sepin-1 adduct (M6, Cys–sepin-1) and one GSH–sepin-1 adduct (M7, GSH–sepin-1), were identified in HLM.

TABLE 1 | Summary of metabolites of sepin-1 in liver microsomes.

RT (min)	Observed *m/z* [M+H]	Calculated *m/z* [M+H]	Mass error (ppm)	Predicted molecular formula	Metabolite ID	Source
4.25	224.0675	224.0671	1.8	$C_9H_{10}N_3O_4$	Sepin-1	ND
4.78	194.0929	194.0930	−0.5	$C_9H_{12}N_3O_2$	M1	HLM, MLM, RLM
1.98	194.0927	194.0930	−1.5	$C_9H_{12}N_3O_2$	M2	HLM, MLM, RLM
6.51	385.1618	385.1624	−1.6	$C_{18}H_{20}N_6O_4$	M3	HLM, MLM, RLM
5.82	385.1613	385.1624	−2.8	$C_{18}H_{20}N_6O_4$	M4	HLM, MLM, RLM
6.50	385.1613	385.1624	−2.8	$C_{18}H_{20}N_6O_4$	M5	HLM, MLM, RLM
3.24	313.0961	313.0971	−3.2	$C_{12}H_{16}N_4O_4S$	M6	HLM, MLM, RLM
1.75	499.1608	499.1611	−0.6	$C_{19}H_{26}N_6O_8S$	M7	HLM, MLM, RLM

ND, not detected.

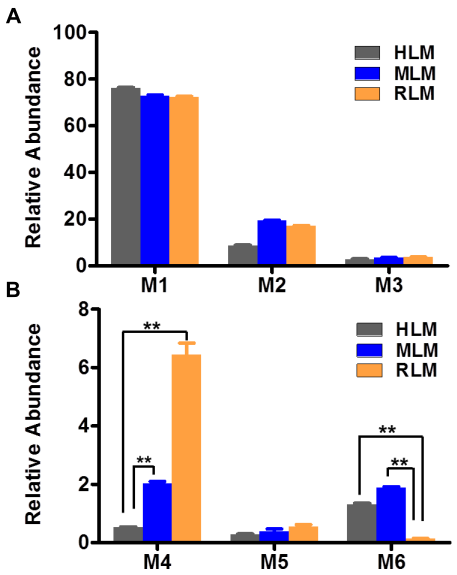

FIGURE 1 | Relative abundance of metabolites in human, mouse, and RLM (HLM, MLM, and RLM), respectively. Quadruplicate incubations for HLM and triplicate incubations for MLM and RLM were carried out in 1× PBS (pH 7.4) containing sepin-1 (30 μM), HLM (1.0 mg/ml), MLM (1.0 mg/ml), or RLM, with or without NADPH (1.0 mM). The metabolites were measured by UHPLC–QTOFMS. The overall abundance of metabolites was set as 100% in each sample. The data are expressed as mean and SEM (n = 3 or 4). **(A)** Relative abundance of major metabolites, M1–M3. **(B)** Relative abundance of minor metabolites, M4–M6. $^{**}p < 0.01$.

Identification of Reduced Metabolites (M1 and M2) in Sepin-1 Metabolism

In the incubation of sepin-1 in HLM, two major reduced metabolites (M1 and M2) were observed and characterized (**Figure 2**). The formation of metabolites M1 and M2 is NADPH dependent (**Figure 2A**). M1 was eluted at 4.78 min (**Figure 2A**), having a protonated molecule [M+H] at m/z = 194 Da (**Figure 2B**). The MS/MS of M1 produced the major fragment ions at m/z 177, 162, and 148, and the fragment ions have been interpreted in the inlaid structural diagram (**Figure 2B**). The structure of M1 was confirmed by comparison with the retention time and MS/MS fragment pattern of a synthesized standard compound (Supplementary Figure S3). M2 was eluted at 1.98 min (**Figure 2A**), having a protonated molecule [M+H] at m/z = 194 (**Figure 2C**). The MS/MS of M2 produced the major fragment ions at m/z 177, 162, and 147. The fragmental ions have been interpreted in the inlaid structural diagram (**Figure 2C**).

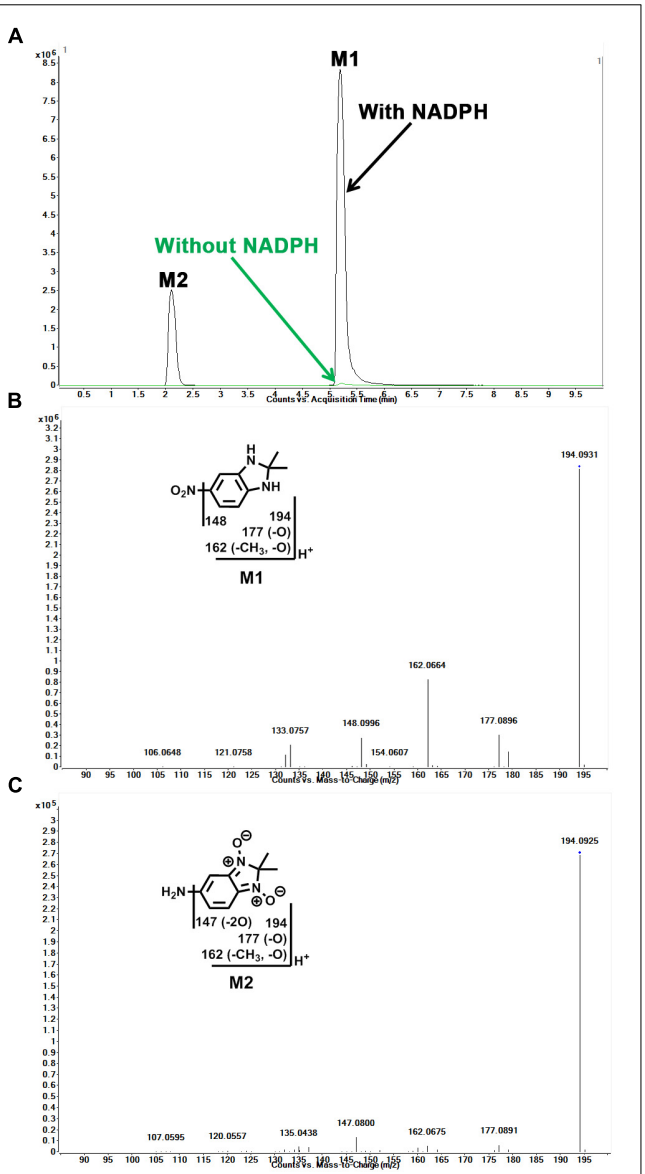

FIGURE 2 | Identification of reduced metabolites (M1 and M2) in HLM. Incubation of sepin-1 was conducted as described in **Figure 1**. The metabolites were analyzed using UHPLC–QTOFMS. Structural elucidations were performed based on accurate mass measurement (mass errors <10 ppm) and MS/MS fragmentations. MS/MS fragmentation was conducted with collision energy ramping from 10 to 45 V. The major daughter ions are interpreted in the inlaid structural diagrams. **(A)** The chromatograms of metabolites M1 and M2. **(B)** The MS/MS of M1. **(C)** The MS/MS of M2.

Identification of Dimer Metabolites (M3, M4, and M5) in Sepin-1 Metabolism

In our study, we found dimer metabolites (M3–M5) formed in HLM, MLM, and RLM. Metabolite M4 is the most abundant dimer in RLM (**Figure 1B**). The dimer formation is NADPH dependent. The formation of dimer metabolites indicated that molecular interaction occurred post-metabolism. The dimer metabolites M3, M4, and M5 were identified by MS/MS and their accurate masses. M3, eluted at 5.82 min (**Figure 3A**), had a protonated molecule $[M+H]^+$ at m/z = 385. The fragmental ions at m/z 339 suggested denitration. The other fragmental ions at m/z 324 and 263 are interpreted in the inlaid structural diagram (**Figure 3B**). M4, eluted at 4.25 min (**Figure 3A**), had a protonated molecule $[M+H]^+$at m/z = 385. The fragmental ions at m/z 339 and 324 have been interpreted in the inlaid structural diagram (**Figure 3C**). M5, eluted

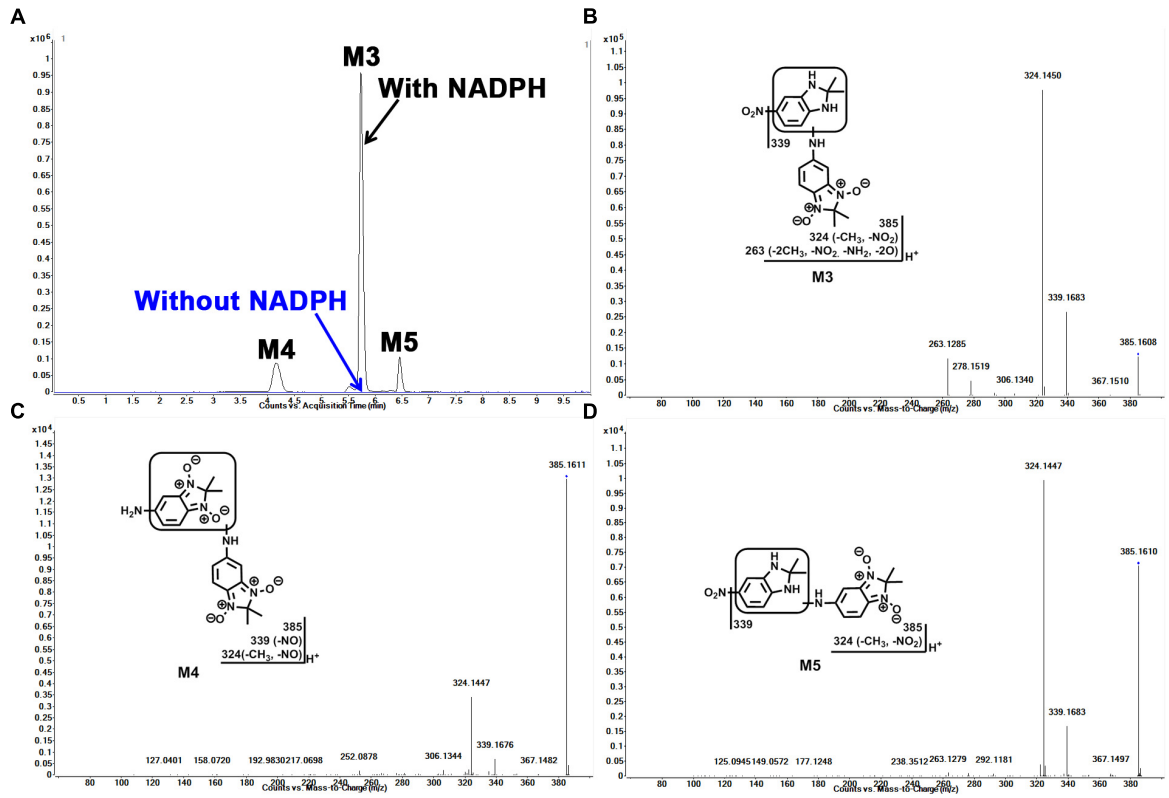

FIGURE 3 | Identification of dimer metabolites (M3, M4, and M5) in HLM. Quadruplicate incubations were performed in 1× PBS (pH 7.4) containing sepin-1 (30 μM), HLM (1.0 mg/ml), with or without NADPH (1.0 mM). The metabolites were analyzed using UHPLC–QTOFMS. The metabolite elucidation conditions are described in **Figure 2**. **(A)** Chromatograms of M3, M4, and M5. **(B)** MS/MS of M3. **(C)** MS/MS of M4. **(D)** MS/MS of M5.

at 6.50 min (**Figure 3A**), also had a protonated molecule $[M+H]^+$ at m/z = 385. The fragmental ions at m/z 339 suggested that denitration has occurred. The other fragmental ion at m/z 324 is interpreted in the inlaid structural diagram (**Figure 3D**).

Identification of Cys–Sepin-1 Adduct (M6) and GSH–Sepin-1 Adduct (M7) in Sepin-1 Metabolism

In HLM, we observed the formation of Cys–sepin-1 (M6). The conjugation of sepin-1 with cysteine suggested that sepin-1 could be bioactivated to form the reactive metabolites in the incubation system. In HLM, in the presence of GSH, we observed GSH–sepin-1 adduct (M7) as expected and identified it with its accurate mass by MS/MS. Our studies suggest that the formation of Cys–sepin-1 and GSH–sepin-1 adducts is NADPH dependent (data not shown). M6, eluted at 3.24 min (**Figure 4A**), had a protonated molecule $[M+H]^+$ at m/z = 313. The fragmental ions of M6 at m/z 267, 252, 224, and 192 were interpreted in the inlaid structural diagram (**Figure 4B**). M7, eluted at 1.75 min (**Figure 4C**), had a protonated molecule $[M+H]^+$ at m/z = 499. The major fragment ion of M7 at m/z 424, 370, and 309 is interpreted in the inlaid structural diagram (**Figure 4D**).

The Role of CYP450s in Sepin-1 Metabolism

Incubation of sepin-1 with different human cDNA-expressed P450s (control, CYP1A2, 2A6, 2B6, 2C8, 2C9, 2C19, 2D6, 2E1, and CYP3A4) revealed that multiple enzymes are involved in the formation of M1–M5 (**Table 2**). CYP3A and CYP2D6 are primary enzymes contributing to the formation of metabolites M2–M5. The formation of M1 is almost equally mediated by different enzyme isoforms (**Table 2**).

Inhibitory Effect of Sepin-1 on CYP450s

The inhibitory effects of sepin-1 on seven main CYP450 isoforms (CYP1A2, 2B6, 2C8, 2C9, 2C19, 2D6, and 3A4) were evaluated. The specific metabolites, acetaminophen for CYP1A2, 8-*O*-efavirenz for CYP2B6, 6-*O*-paclitaxel for CYP2C8, 4-*O*-diclofenac for 2C9, 4-*O*-mephenytoin for 2C19, dextromethorphan *O*-demethylation for 2D6, and 1-*O*-midazolam for 3A4, were monitored by LC–MS/MS. Our data suggested that the IC_{50}s of sepin-1 on CYP1A2 (8.1 μM), CYP2C19 (8.9 μM), and CYP3A4 (8.7 μM) are less than 10 μM (**Figures 5A,E,G**), whereas IC_{50}s on CYP2B6 (14.5 μM), CYP2C8 (17.8 μM), CYP2C9 (21.3 μM), and CYP2D6 (42.5 μM) are greater than 10 μM (**Figures 5B–D,F**).

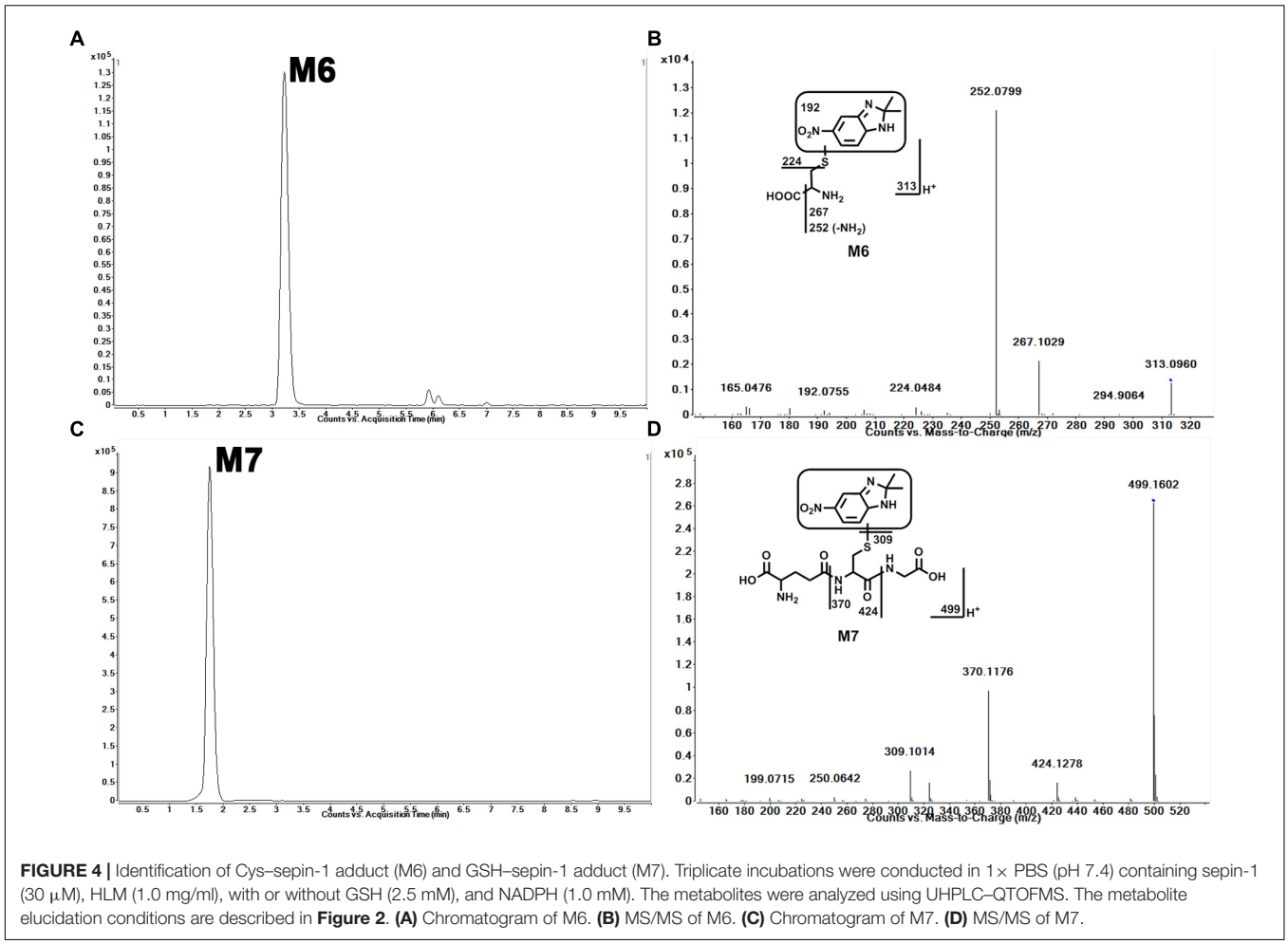

FIGURE 4 | Identification of Cys–sepin-1 adduct (M6) and GSH–sepin-1 adduct (M7). Triplicate incubations were conducted in 1× PBS (pH 7.4) containing sepin-1 (30 μM), HLM (1.0 mg/ml), with or without GSH (2.5 mM), and NADPH (1.0 mM). The metabolites were analyzed using UHPLC–QTOFMS. The metabolite elucidation conditions are described in **Figure 2**. **(A)** Chromatogram of M6. **(B)** MS/MS of M6. **(C)** Chromatogram of M7. **(D)** MS/MS of M7.

TABLE 2 | Role of P450s in the metabolism of sepin-1.

	M1	M2	M3	M4	M5
Control	79.5	41.5	17.0	20.3	19.0
CYP1A2	86.3	50.5	36.8	40.2	16.5
CYP2A6	90.8	76.1	51.0	59.6	14.5
CYP2B6	91.9	85.9	59.0	55.0	19.1
CYP2C8	91.3	63.6	52.0	53.5	28.2
CYP2C9	90.4	57.2	53.0	51.4	24.5
CYP2C19	90.8	67.5	49.1	60.4	23.4
CYP2D6	96.9	100.0	95.5	100.0	20.3
CYP2E1	89.9	53.2	46.8	55.6	28.4
CYP3A4	100.0	95.3	100.0	97.1	100.0

cDNA-expressed P450s were used to determine the role of individual CYP450 in sepin-1 metabolism. The incubation conditions of sepin-1 were detailed in experimental procedures. All samples were analyzed by UHPLC–QTOFMS. The peak area of each metabolite from the incubation with the highest abundance was set as 100%. All data are expressed as mean (n = 2).

DISCUSSION

In this study, we employed a LC–MS-based metabolomic approach to profile sepin-1 (a potent separase inhibitor and an investigational chemotherapeutic drug candidate) metabolism and bioactivation in HLM, MLM, and RLM. Metabolomic approaches could readily screen out the sepin-1-related metabolites and reactive intermediates from the biomatrix (Li et al., 2011, 2012). We identified seven sepin-1 metabolites and adducts, including reduced metabolites M1 and M2, dimer metabolites M3–M5, and cysteine–sepin-1 adduct (Cys–sepin-1) M6 and GSH–sepin-1 adduct M7, using the metabolomic technology. All the metabolites were presented in HLM, MLM, and RLM. M4 was the most abundant dimer in RLM, but only a trace amount was observed in HLM. However, the Cys–sepin-1 adduct M6 was mainly formed in HLM and MLM (**Figure 1B**). M1 and M2 are dominant metabolites in all the three species of HLM, MLM, and RLM (**Figure 1**). Among these metabolites, one Cys–sepin-1 adduct (M6) was detected and characterized. The formation of M6 was also NADPH dependent. In HLM, sepin-1 is metabolized rapidly to the dominant-reduced metabolites M1 and M2. Therefore, the most abundant metabolite M1 was synthesized (Do et al., 2016) and the inhibitory activity of M1 on separase will be assayed next.

The reactive metabolites play a critical role in the pathogenesis of idiosyncratic adverse drug reactions (Attia, 2010;

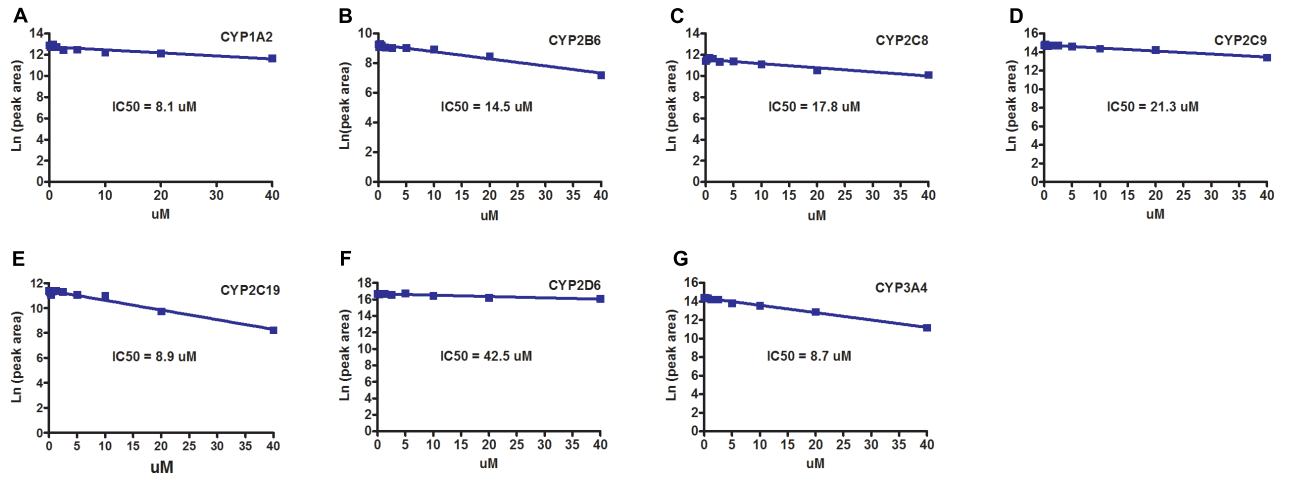

FIGURE 5 | The inhibitory effects of sepin-1 on CYP450s. Incubations were performed in 1× PBS (pH 7.4), containing 0, 0.156, 0.312, 0.625, 1.25, 2.5, 5, 10, 20, or 40 μM sepin-1, 2 pmol of each cDNA-expressed P450 enzymes, and corresponding substrates. The specific metabolites were analyzed using UHPLC–QQQMS. **(A)** Inhibition of CYP1A2. **(B)** Inhibition of CYP2B6. **(C)** Inhibition of CYP2C8. **(D)** Inhibition of CYP2C9. **(E)** Inhibition of CYP2C19. **(F)** Inhibition of CYP2D6. **(G)** Inhibition of CYP3A4.

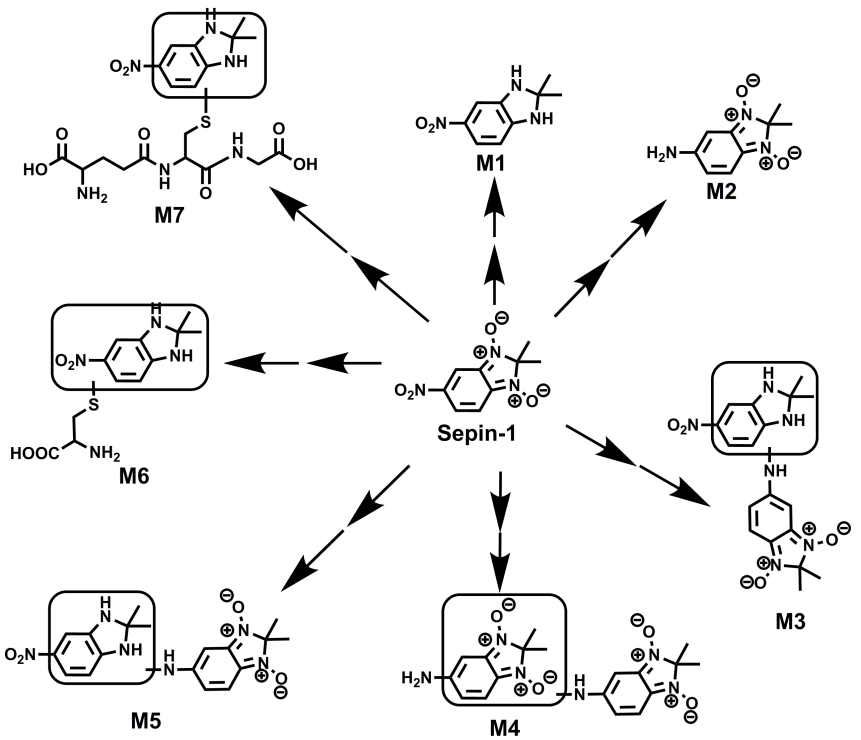

FIGURE 6 | Summary of putative structures of GEF metabolites and adducts. All structures were determined based on the exact mass (mass error <10 ppm) and MS/MS fragments.

Park et al., 2011; Thompson et al., 2016). The formation of Cys–sepin-1 adduct (M6) indicated that sepin-1 could be bioactivated to generate the reactive metabolite in HLM. The mechanism of the formation of Cys–sepin-1 adduct in HLM is not known yet, but the adduct M6 is derived from the major metabolite M1 by conjugating with cysteine in HLM. Reduced GSH is an abundant physiological nucleophile and frequently used to capture soft electrophiles (e.g., epoxides, quinones, quinone imines, and quinone methides) in *in vitro* systems (Evans et al., 2004). Our study revealed one GSH–sepin-1 adduct (M7) in the incubations of sepin-1 in HLM with GSH. Although the mechanisms of formation of GSH–sepin-1 adducts

in HLM are not clear, the formation of GSH–sepin-1 adduct further suggested that the sepin-1 could produce the reactive electrophiles in HLM. Generally, excess reactive electrophiles are capable of covalent binding to protein, DNA, and other biomolecules. It is thought that cellular function is compromised in certain cases, followed by organ toxicity (O'Brien et al., 2005). These reactive metabolites from sepin-1 may induce some adverse effects. In drug development, researchers attempt to reduce the risk factors of toxicity by minimizing the formation of reactive metabolites. This information will be helpful for medicinal chemists to further optimize the structure of sepin-1 to improve its safety. For example, medicinal chemists could decrease the formation of reactive metabolites by blocking their metabolic sites via the structural modifications.

The mechanisms of sepin-1 reduction (M1 and M2) and dimer formation (M3–M5) are not clear yet. The liver microsomes involved in the formation of reduced metabolite is known (Leskovac and Popovic, 1980; Placidi et al., 1993; Wang et al., 2005). Our study suggested that multiple P450s enzymes contribute to sepin-1 metabolism. CYP3A4 and CYP2D6 are the primary enzymes responsible for the generation of metabolites M2–M5 (**Table 2**). For M1, all the test isoenzymes make similar contributions to the formation of M1. Because CYP3A4 is the most abundant drug-metabolizing enzyme in the liver, the formation of M1 should be mainly mediated by CYP3A4. The role of CYP3A4 in the formation of M1 can be investigated further using Cyp3a-null mice. As the GSH–sepin-1 adduct was formed by GSH conjugating with the major metabolite M1, the formation of GSH–sepin-1 could have been mediated by multiple P450 enzymes as well. Other enzymes (e.g., cytochrome b5 reductase in the microsomes) have been reported to be implicated in the reduction of *N*-oxide (Zheng et al., 2011). In addition, the reduction of *N*-oxide (e.g., quinoxaline-1,4-dioxide) could be mediated by aldehyde oxidase and xanthine oxidase in the cytosol as well (Zheng et al., 2011; Mu et al., 2014). The exact role of P450s and reductases in the sepin-1 reduction will be further investigated using CYPP450 inhibitor (1H-benzotriazol-1-amine and carbon monoxide) and the liver microsomes from CYP450 reductase-knock out mice. Non-enzymatic reduction of *N*-oxide by heme of P450 will be tested using the boiled microsomes as well in the future study (Takekawa et al., 2001).

As discussed as above, sepin-1 could be metabolized by multiple enzymes, other drugs thus may have little effect on the metabolism of sepin-1, when sepin-1 is co-administrated. However, sepin-1 may have significant effects on the metabolism of co-administrated drugs and cause drug–drug interactions by inhibiting their major drug-metabolizing enzymes. In the current study, the inhibitory effects of sepin-1 on seven main CYP450 isoenzymes (CYP1A2, 2B6, 2C8, 2C9, 2C19, 2D6, and 3A4) were evaluated. These seven enzymes metabolize >90% of marked drugs. Typically, inhibition potency of a compound can be categorized into three classification bands: (1) potent inhibition with IC_{50} < 1 μM; (2) moderate inhibition with 1 μM < IC_{50} < 10 μM; or (3) no or weak inhibition with IC_{50} > 10 μM [Food and Drug Administration (FDA) draft guide for industry, 2012]. Using the corresponding substrates recommended by FDA and monitoring their specific metabolites by LC–MS/MS, we unraveled that sepin-1 has moderate inhibition on CYP1A2 (IC_{50} = 8.1 μM), CYP2C19 (IC_{50} = 8.9 μM), and CYP3A4 (IC_{50} = 8.7 μM). Our data also indicate that sepin-1 has weak inhibition on CYP 2B6 (IC_{50} = 14.5 μM), CYP2C8 (IC_{50} = 17.8 μM), CYP2C9 (IC_{50} = 21.3 μM), and CYP2D6 (IC_{50} = 42.5 μM). These data suggest that sepin-1 may have some moderate interaction with the drugs mainly metabolized by CYP1A2, 2C19, and/or CYP3A4. For example, GEF, a tyrosine kinase inhibitor, is mainly metabolized by CYP3A4 (Liu et al., 2015). The pharmacokinetics of GEF may be moderately altered by sepin-1 if GEF is taken together with sepin-1. In the current study, we only evaluated the co-incubation of sepin-1 and enzyme substrates to evaluate the inhibitory effects of sepin-1. The metabolism-/mechanism-based inhibition was not performed here.

In summary, the metabolism of sepin-1 in HLM, MLM, and RLM was extensively studied using LC–MS-based metabolomic approaches. This study identified a total of seven metabolites and adducts related to sepin-1 (**Figure 6**) including Cys–sepin-1 and GSH–sepin-1 adducts. The enzyme contributing to the formation of sepin-1 metabolism was identified using recombinant P450 isoenzymes. Additionally, the inhibitory effects of sepin-1 on the seven main CYP450 isoenzymes were evaluated. This study provides the foundation for optimizing the structures and predicting the possible drug–drug interactions from the metabolic prospective of sepin-1, our lead separase inhibitor for cancer therapy. Further studies are suggested to illustrate the role of other enzymes contributing to reduced metabolites of sepin-1, metabolism of sepin-1 *in vivo*, and the inductive effects of sepin-1 on CYP450 isoenzymes *in vitro* and *in vivo*.

AUTHOR CONTRIBUTIONS

DP and FL participated in the research design. NZ, SG, SRG, and FL conducted the experiments. FL performed the data analysis. DP, NZ, and FL wrote or contributed to the writing of the manuscript.

FUNDING

This work was supported by the Cancer Prevention and Research Institute of Texas Grant No. DP150064, Department of Defense Award W81XWH-15-1-0122, and Alkek Award for Pilot Projects in Experimental Therapeutics to DP; the Eunice Kennedy Shriver National Institute of Child Health and Human Development (P01 HD087157-01A1) and Cancer Prevention & Research Institute of Texas (RP160805) to Dr. Martin M. Matzuk; and SG was supported by Alex Lemonade Stand Foundation Pediatric Oncology Student Training (POST) Award.

SUPPLEMENTARY MATERIAL

The Supplementary Material for this article can be found online at: https://www.frontiersin.org/articles/10.3389/fphar.2018.00313/full#supplementary-material

REFERENCES

Attia, S. M. (2010). Deleterious effects of reactive metabolites. *Oxid. Med. Cell. Longev.* 3, 238–253. doi: 10.4161/oxim.3.4.13246

Bai, X., and Bembenek, J. N. (2017). Protease dead separase inhibits chromosome segregation and RAB-11 vesicle trafficking. *Cell Cycle* 16, 1902–1917. doi: 10.1080/15384101.2017.1363936

Bembenek, J. N., Richie, C. T., Squirrell, J. M., Campbell, J. M., Eliceiri, K. W., Poteryaev, D., et al. (2007). Cortical granule exocytosis in *C. elegans* is regulated by cell cycle components including separase. *Development* 134, 3837–3848. doi: 10.1242/dev.011361

Ciosk, R., Zachariae, W., Michaelis, C., Shevchenko, A., Mann, M., and Nasmyth, K. (1998). An ESP1/PDS1 complex regulates loss of sister chromatid cohesion at the metaphase to anaphase transition in yeast. *Cell* 93, 1067–1076. doi: 10.1016/S0092-8674(00)81211-8

Do, H. T., Zhang, N., Pati, D., and Gilbertson, S. R. (2016). Synthesis and activity of benzimidazole-1,3-dioxide inhibitors of separase. *Bioorg. Med. Chem. Lett.* 26, 4446–4450. doi: 10.1016/j.bmcl.2016.07.080

Evans, D. C., Watt, A. P., Nicoll-Griffith, D. A., and Baillie, T. A. (2004). Drug-protein adducts: an industry perspective on minimizing the potential for drug bioactivation in drug discovery and development. *Chem. Res. Toxicol.* 17, 3–16. doi: 10.1021/tx034170b

Gorr, I. H., Boos, D., and Stemmann, O. (2005). Mutual inhibition of separase and Cdk1 by two-step complex formation. *Mol. Cell.* 19, 135–141. doi: 10.1016/j.molcel.2005.05.022

Holland, A. J., and Taylor, S. S. (2006). Cyclin-B1-mediated inhibition of excess separase is required for timely chromosome disjunction. *J. Cell Sci.* 119, 3325–3336. doi: 10.1242/jcs.03083

Lee, K., and Rhee, K. (2012). Separase-dependent cleavage of pericentrin B is necessary and sufficient for centriole disengagement during mitosis. *Cell Cycle* 11, 2476–2485. doi: 10.4161/cc.20878

Leskovac, V., and Popovic, M. (1980). Mechanism of reduction of nitrofurantoin on liver microsomes. *Pharmacol. Res. Commun.* 12, 13–27. doi: 10.1016/S0031-6989(80)80058-0

Li, F., Gonzalez, F. J., and Ma, X. (2012). LC–MS-based metabolomics in profiling of drug metabolism and bioactivation. *Acta Pharm. Sin. B* 2, 118–125. doi: 10.1016/j.apsb.2012.02.010

Li, F., Lu, J., and Ma, X. (2011). Profiling the reactive metabolites of xenobiotics using metabolomic technologies. *Chem. Res. Toxicol.* 24, 744–751. doi: 10.1021/tx200033v

Li, F., Lu, J., and Ma, X. (2014). CPY3A4-mediated alpha-hydroxyaldehyde formation in saquinavir metabolism. *Drug Metab. Dispos.* 42, 213–220. doi: 10.1124/dmd.113.054874

Lin, Z., Luo, X., and Yu, H. (2016). Structural basis of cohesin cleavage by separase. *Nature* 532, 131–134. doi: 10.1038/nature17402

Liu, X., Lu, Y., Guan, X., Dong, B., Chavan, H., Wang, J., et al. (2015). Metabolomics reveals the formation of aldehydes and iminium in gefitinib metabolism. *Biochem. Pharmacol.* 97, 111–121. doi: 10.1016/j.bcp.2015.07.010

Liu, X., Lu, Y. F., Guan, X., Zhao, M., Wang, J., and Li, F. (2016). Characterizing novel metabolic pathways of melatonin receptor agonist agomelatine using metabolomic approaches. *Biochem. Pharmacol.* 109, 70–82. doi: 10.1016/j.bcp.2016.03.020

Matsuo, K., Ohsumi, K., Iwabuchi, M., Kawamata, T., Ono, Y., and Takahashi, M. (2012). Kendrin is a novel substrate for separase involved in the licensing of centriole duplication. *Curr. Biol.* 22, 915–921. doi: 10.1016/j.cub.2012.03.048

McAleenan, A., Clemente-Blanco, A., Cordon-Preciado, V., Sen, N., Esteras, M., Jarmuz, A., et al. (2013). Post-replicative repair involves separase-dependent removal of the kleisin subunit of cohesin. *Nature* 493, 250–254. doi: 10.1038/nature11630

Meyer, R., Fofanov, V., Panigrahi, A., Merchant, F., Zhang, N., and Pati, D. (2009). Overexpression and mislocalization of the chromosomal segregation protein separase in multiple human cancers. *Clin. Cancer Res.* 15, 2703–2710. doi: 10.1158/1078-0432.CCR-08-2454

Moschou, P. N., Savenkov, E. I., Minina, E. A., Fukada, K., Reza, S. H., Gutierrez-Beltran, E., et al. (2016). EXTRA SPINDLE POLES (Separase) controls anisotropic cell expansion in Norway spruce (*Picea abies*) embryos independently of its role in anaphase progression. *New Phytol.* 212, 232–243. doi: 10.1111/nph.14012

Moschou, P. N., Smertenko, A. P., Minina, E. A., Fukada, K., Savenkov, E. I., Robert, S., et al. (2013). The caspase-related protease separase (extra spindle poles) regulates cell polarity and cytokinesis in *Arabidopsis*. *Plant Cell* 25, 2171–2186. doi: 10.1105/tpc.113.113043

Mu, P., Zheng, M., Xu, M., Zheng, Y., Tang, X., Wang, Y., et al. (2014). N-oxide reduction of quinoxaline-1,4-dioxides catalyzed by porcine aldehyde oxidase SsAOX1. *Drug Metab. Dispos.* 42, 511–519. doi: 10.1124/dmd.113.055418

Mukherjee, M., Byrd, T., Brawley, V. S., Bielamowicz, K., Li, X. N., Merchant, F., et al. (2014a). Overexpression and constitutive nuclear localization of cohesin protease Separase protein correlates with high incidence of relapse and reduced overall survival in glioblastoma multiforme. *J. Neurooncol.* 119, 27–35. doi: 10.1007/s11060-014-1458-6

Mukherjee, M., Ge, G., Zhang, N., Edwards, D. G., Sumazin, P., Sharan, S. K., et al. (2014b). MMTV-Espl1 transgenic mice develop aneuploid, estrogen receptor alpha (ERalpha)-positive mammary adenocarcinomas. *Oncogene* 33, 5511–5522. doi: 10.1038/onc.2013.493

Nagao, K., Adachi, Y., and Yanagida, M. (2004). Separase-mediated cleavage of cohesin at interphase is required for DNA repair. *Nature* 430, 1044–1048. doi: 10.1038/nature02803

Nakamura, A., Arai, H., and Fujita, N. (2009). Centrosomal Aki1 and cohesin function in separase-regulated centriole disengagement. *J. Cell Biol.* 187, 607–614. doi: 10.1083/jcb.200906019

O'Brien, P. J., Siraki, A. G., and Shangari, N. (2005). Aldehyde sources, metabolism, molecular toxicity mechanisms, and possible effects on human health. *Crit. Rev. Toxicol.* 35, 609–662. doi: 10.1080/10408440591002183

Park, B. K., Boobis, A., Clarke, S., Goldring, C. E., Jones, D., Kenna, J. G., et al. (2011). Managing the challenge of chemically reactive metabolites in drug development. *Nat. Rev. Drug Discov.* 10, 292–306. doi: 10.1038/nrd3408

Pati, D. (2008). Oncogenic activity of separase. *Cell Cycle* 7, 3481–3482. doi: 10.4161/cc.7.22.7048

Placidi, L., Cretton, E. M., Placidi, M., and Sommadossi, J. P. (1993). Reduction of 3'-azido-3'-deoxythymidine to 3'-amino-3'-deoxythymidine in human liver microsomes and its relationship to cytochrome P450. *Clin. Pharmacol. Ther.* 54, 168–176. doi: 10.1038/clpt.1993.128

Richie, C. T., Bembenek, J. N., Chestnut, B., Furuta, T., Schumacher, J. M., Wallenfang, M., et al. (2011). Protein phosphatase 5 is a negative regulator of separase function during cortical granule exocytosis in *C. elegans*. *J. Cell Sci.* 124, 2903–2913. doi: 10.1242/jcs.073379

Schockel, L., Mockel, M., Mayer, B., Boos, D., and Stemmann, O. (2011). Cleavage of cohesin rings coordinates the separation of centrioles and chromatids. *Nat. Cell Biol.* 13, 966–972. doi: 10.1038/ncb2280

Stemmann, O., Zou, H., Gerber, S. A., Gygi, S. P., and Kirschner, M. W. (2001). Dual inhibition of sister chromatid separation at metaphase. *Cell* 107, 715–726. doi: 10.1016/S0092-8674(01)00603-1

Takekawa, K., Kitamura, S., Sugihara, K., and Ohta, S. (2001). Non-enzymatic reduction of aliphatic tertiary amine N-oxides mediated by the haem moiety of cytochrome P450. *Xenobiotica* 31, 11–23. doi: 10.1080/00498250010024997

Thompson, R. A., Isin, E. M., Ogese, M. O., Mettetal, J. T., and Williams, D. P. (2016). Reactive metabolites: current and emerging risk and hazard assessments. *Chem. Res. Toxicol.* 29, 505–533. doi: 10.1021/acs.chemrestox.5b00410

Tsou, M. F., Wang, W. J., George, K. A., Uryu, K., Stearns, T., and Jallepalli, P. V. (2009). Polo kinase and separase regulate the mitotic licensing of centriole duplication in human cells. *Dev. Cell* 17, 344–354. doi: 10.1016/j.devcel.2009.07.015

Uhlmann, F., Wernic, D., Poupart, M. A., Koonin, E. V., and Nasmyth, K. (2000). Cleavage of cohesin by the CD clan protease separin triggers anaphase in yeast. *Cell* 103, 375–386. doi: 10.1016/S0092-8674(00)00130-6

Viadiu, H., Stemmann, O., Kirschner, M. W., and Walz, T. (2005). Domain structure of separase and its binding to securin as determined by EM. *Nat. Struct. Mol. Biol.* 12, 552–553. doi: 10.1038/nsmb935

Wang, Y. P., Yan, J., Fu, P. P., and Chou, M. W. (2005). Human liver microsomal reduction of pyrrolizidine alkaloid N-oxides to form the corresponding carcinogenic parent alkaloid. *Toxicol. Lett.* 155, 411–420. doi: 10.1016/j.toxlet.2004.11.010

Winter, A., Schmid, R., and Bayliss, R. (2015). Structural insights into separase architecture and substrate recognition through computational modelling of

caspase-like and death domains. *PLoS Comput. Biol.* 11:e1004548. doi: 10.1371/journal.pcbi.1004548

Zhang, N., Ge, G., Meyer, R., Sethi, S., Basu, D., Pradhan, S., et al. (2008). Overexpression of Separase induces aneuploidy and mammary tumorigenesis. *Proc. Natl. Acad. Sci. U.S.A.* 105, 13033–13038. doi: 10.1073/pnas.0801610105

Zhang, N., and Pati, D. (2017). Biology and insights into the role of cohesin protease separase in human malignancies. *Biol. Rev. Camb. Philos. Soc.* 92, 2070–2083. doi: 10.1111/brv.12321

Zhang, N., Scorsone, K., Ge, G., Kaffes, C. C., Dobrolecki, L. E., Mukherjee, M., et al. (2014). Identification and characterization of separase inhibitors (Sepins) for cancer therapy. *J. Biomol. Screen.* 19, 878–889. doi: 10.1177/1087057114520972

Zheng, M., Jiang, J., Wang, J., Tang, X., Ouyang, M., and Deng, Y. (2011). The mechanism of enzymatic and non-enzymatic N-oxide reductive metabolism of cyadox in pig liver. *Xenobiotica* 41, 964–971. doi: 10.3109/00498254.2011.593207

Zou, H., McGarry, T. J., Bernal, T., and Kirschner, M. W. (1999). Identification of a vertebrate sister-chromatid separation inhibitor involved in transformation and tumorigenesis. *Science* 285, 418–422. doi: 10.1126/science.285.5426.418

Conflict of Interest Statement: The authors declare that the research was conducted in the absence of any commercial or financial relationships that could be construed as a potential conflict of interest.